2014 IEEE International Conference on Robotics & Automation (ICRA)
Hong Kong Convention and Exhibition Center
May 31 - June 7, 2014. Hong Kong, China

A Continuous Dynamic Model for an Omnidirectional Mobile Robot

Chao Ren[1] and Shugen Ma[2]

***Abstract*— The omnidirectional mobile robots with MY wheels-II are discontinuous dynamic systems. This paper derives a continuous model from a given discontinuous dynamic model. Firstly, the problem of a previously proposed dynamic model, average dynamic model, is analyzed. It shows that the effectiveness of the average dynamic model is limited to robots under a certain class of configurations. To overcome this problem, we first derive the switching conditions of MY wheel-II. Then a continuous dynamic modeling method, using adaptive continuous curves instead of the real discontinuous contact radius in the discontinuous dynamic model, is proposed based on the switching conditions. The resulting dynamic model is a smooth NLPV model, which may then be used as one solution for the model-based control design. The effectiveness of the proposed NLPV model is verified and compared through open-loop simulations against the average model.**

I. INTRODUCTION

Recently, omnidirectional mobile robots (OMRs) are becoming increasingly popular in many applications, especially in the narrow spaces, since they can perform translational and rotational motion independently and simultaneously.

Various omnidirectional wheel mechanisms were proposed in the past few decades. In our previous work [1], we classified these wheel mechanisms into two groups, namely, "non-switch wheels" and "switch wheels". The classification depends on whether the contact radius of the robot switches during the robot motion. The contact radius is the distance between mass center of the robot and the wheel contact point with ground. Many omnidirectional wheels are "non-switch wheels", such as Mecanum wheel [2], Alternate wheel [3] and Ball wheel [4], [5]. For non-switch wheeled OMRs, the contact radius of the wheel to the center of gravity of the robot is constant. On the other hand, by far, the proposed "switch wheels" are shown in Fig. 1. They are Longitudinal orthogonal-wheel [6], MY wheel [7], MY wheel-II [8], Swedish wheel [9] and Omni-wheel [10]. Switch wheeled OMRs have the advantages such as, smooth contact with the ground [6] and higher payload ability [7]. Specially, the MY wheel-II mechanism is more insensitive to the fragments on the ground. However, these five mechanisms have a common feature, i.e., the contact radius of the wheel to the center of gravity of the robot switches. The dynamics of the non-switch wheeled OMRs is smooth nonlinear while the switch wheeled OMRs are switched nonlinear systems (hybrid systems), i.e., the robot dynamics is discontinuous due to the switching effects [1].

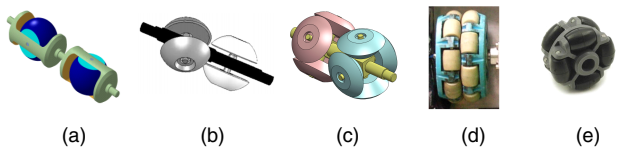

Fig. 1. Switch wheel mechanisms: (a) Longitudinal orthogonal-wheel. (b) MY wheel. (c) MY wheel-II. (d) Swedish wheel. (e) Omni-wheel.

The tracking controller design based on the discontinuous dynamic model is still an open problem, since the switch wheeled OMRs are autonomous switched nonlinear dynamic systems [11], [12]. On the other hand, most of the analysis and control design methods in the literature are based on the continuous dynamic models. Thereby, the continuous dynamic modeling for the switch wheeled OMRs is indeed expected. In fact, this idea is widely employed in the control of hybrid systems [13], while the modeling errors are considered as the perturbation of the closed-loop system. In [1], we proposed an average dynamic modeling method for an OMR with MY wheels-II, which results in a smooth nonlinear dynamic model.

In this paper, a continuous nonlinear parameter varying (NLPV) model is derived from a given discontinuous model. First, a brief analysis of the average model is presented. It shows that the effectiveness of the average dynamic model is limited to robots under a certain class of configurations. Then the switching conditions of the MY wheel-II mechanism are analyzed. Based on the derived switching conditions, a NLPV model is derived to overcome the limitations of the average dynamic modeling method. Its key idea is to design adaptive continuous curves to approach the real discontinuous contact radius. The obtained adaptive curves are then used instead of the real contact radius in the discontinuous dynamic model. Finally, open loop simulations show that the NLPV model is much more accurate in predicting the responses of the discontinuous model, than the average model.

The remainder of this paper is organized as follows. In Section II, the discontinuous dynamic model is derived. The problem of the average dynamic modeling method is also analyzed. In Section III, the NLPV dynamic model is presented. Simulations are presented in Section IV. Finally, conclusions are drawn in Section V.

[1]C. Ren is with Department of Robotics, Ritsumeikan University, 525-8577, Shiga, Japan gr0119vp@ed.ritsumei.ac.jp

[2]S. Ma is with Department of Robotics, Ritsumeikan University, 525-8577, Shiga, Japan. He is also with School of Electrical Engineering and Automation, Tianjin University, 300072, Tianjin, China shugen.ma@ieee.org

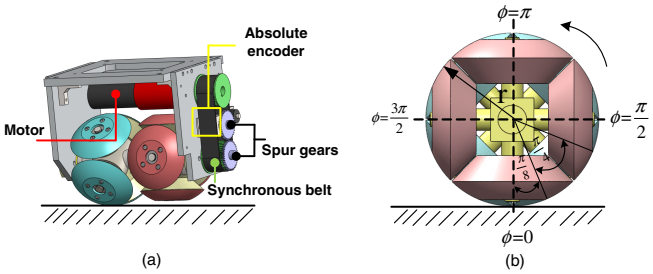

Fig. 2. (a) MY wheel-II assembly. (b) End view.

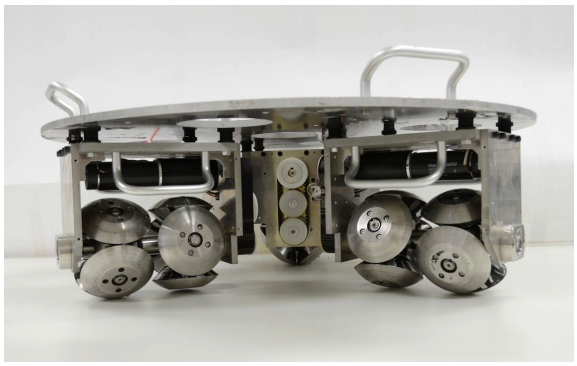

Fig. 3. Prototype platform

II. DYNAMIC MODELING

A. Prototype Platform

The MY wheel-II mechanism assembly and its end-view are shown in Fig. 2. It can be seen from Fig. 2(a) that each wheel has two contact points with the ground. The two contact points switch between the two sets of crowns whenever the wheel turns $\frac{\pi}{4}$, and therefore eight switches occur during each turn (see Fig. 2(b)). Attention should be paid to the absolute encoder installed in each assembly, which is used to detect the switching of the contact radius (see Fig. 2(a)). If odometry is employed in the positioning of switch wheeled OMRs, the absolute encoder is indispensable. The prototype platform is shown in Fig. 3, with three MY wheel-II assemblies arranged with a 120° interval angle underneath the steel disk. For a detailed description of the MY wheel-II mechanism and the prototype platform, the readers are referred to [8].

B. Discontinuous Dynamic Model

There are two coordinate frames used in the modeling (Fig. 4): the world coordinate frame $\{W\}$ fixed on the ground and the moving coordinate frame $\{M\}$ fixed on the robot mass center.

The coordinate transformation matrix from the moving coordinate frame to the world coordinate frame is as follows:

$$ {}^{W}_{M}\mathbf{R} = \begin{bmatrix} \cos\theta & -\sin\theta & 0 \\ \sin\theta & \cos\theta & 0 \\ 0 & 0 & 1 \end{bmatrix} \tag{1} $$

The discontinuous dynamic model including the motor dynamic was presented in our previous work [1]. The de-

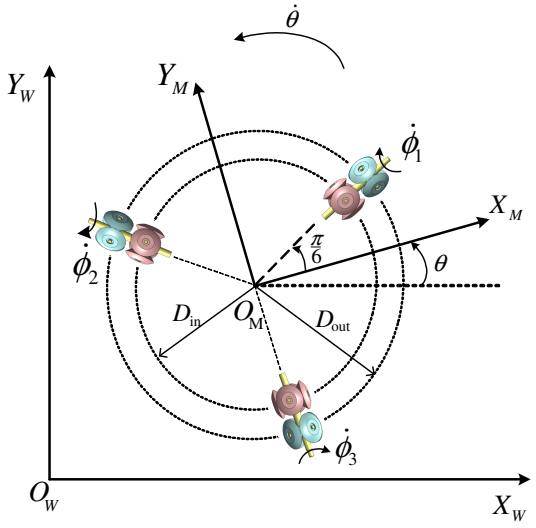

Fig. 4. Coordinate frames of the omnidirectional mobile robot.

veloped dynamic model is similar to those in [14], [15]. The robot dynamic model in the world coordinate frame can be obtained as [1]:

$$ \mathbf{M}\ddot{\mathbf{q}} + \mathbf{C}\dot{\mathbf{q}} = \mathbf{B}\mathbf{u} \tag{2} $$

where

$$ \mathbf{M} = \mathbf{M}_2 {}^{W}_{M}\mathbf{R}^T,\ \mathbf{C} = \mathbf{C}_2 {}^{W}_{M}\mathbf{R}^T - \mathbf{M}_2 {}^{W}_{M}\mathbf{R}^T {}^{W}_{M}\dot{\mathbf{R}} {}^{W}_{M}\mathbf{R}^T,\ \mathbf{B} = \mathbf{B}_2 $$

$$ \mathbf{M}_2 = \begin{bmatrix} \frac{3}{2}p_0 + m & 0 & p_0(-\frac{L_1+L_2-2L_3}{2}) \\ 0 & \frac{3}{2}p_0 + m & \frac{\sqrt{3}}{2}p_0(L_1 - L_2) \\ p_0(-\frac{L_1+L_2-2L_3}{2}) & \frac{\sqrt{3}}{2}p_0(L_1 - L_2) & p_0(L_1^2 + L_2^2 + L_3^2) + I_v \end{bmatrix} $$

$$ \mathbf{C}_2 = \begin{bmatrix} \frac{3}{2}p_1 & -m\dot{\theta} & p_1(-\frac{L_1+L_2-2L_3}{2}) \\ m\dot{\theta} & \frac{3}{2}p_1 & \frac{\sqrt{3}}{2}p_1(L_1 - L_2) \\ p_1(-\frac{L_1+L_2-2L_3}{2}) & \frac{\sqrt{3}}{2}p_1(L_1 - L_2) & p_1(L_1^2 + L_2^2 + L_3^2) \end{bmatrix} $$

$$ \mathbf{B}_2 = p_2 \begin{bmatrix} -\frac{1}{2} & -\frac{1}{2} & 1 \\ \frac{\sqrt{3}}{2} & -\frac{\sqrt{3}}{2} & 0 \\ L_1 & L_2 & L_3 \end{bmatrix} $$

$$ \mathbf{u} = \begin{bmatrix} u_1 & u_2 & u_3 \end{bmatrix}^{\mathrm{T}} $$

$p_0 = \frac{n^2 I_0}{r^2}$, $p_1 = \frac{n^2}{r^2}(b_0 + \frac{k_t k_b}{R_a})$, $p_2 = \frac{nk_t}{rR_a}$,

and $\mathbf{q} = \begin{bmatrix} x & y & \theta \end{bmatrix}^T$ is robot location and orientation angle in the world frame, r is the wheel radius (see Fig. 2(b)), L_i is the contact radius of each assembly, $i = 1,2,3$,

$$ L_i = \begin{cases} D_{in}, & if\ \frac{\pi}{8} + \frac{n\pi}{2} < \phi_i \le \frac{3\pi}{8} + \frac{n\pi}{2} \\ D_{out}, & if\ -\frac{\pi}{8} + \frac{n\pi}{2} < \phi_i \le \frac{\pi}{8} + \frac{n\pi}{2} \end{cases} \quad n = 0, \pm 1, \pm 2, \ldots \tag{3} $$

and D_{in} and D_{out} are the inner and outer contact radius, respectively, ϕ_i is the angular position of the wheel. u_i is the applied motor voltage, m is the robot mass, R_a is the armature resistance, k_b is the motor back emf constant, k_t is

TABLE I

CONTACT MODES OF THE THREE-WHEELED MOBILE ROBOT

L_1, L_2, L_3	D_{in}, D_{in}, D_{in}	D_{in}, D_{in}, D_{out}	D_{in}, D_{out}, D_{in}	D_{in}, D_{out}, D_{out}
Contact Mode	Mode 1	Mode 2	Mode 3	Mode 4
L_1, L_2, L_3	D_{out}, D_{in}, D_{in}	D_{out}, D_{in}, D_{out}	D_{out}, D_{out}, D_{in}	$D_{out}, D_{out}, D_{out}$
Contact Mode	Mode 5	Mode 6	Mode 7	Mode 8

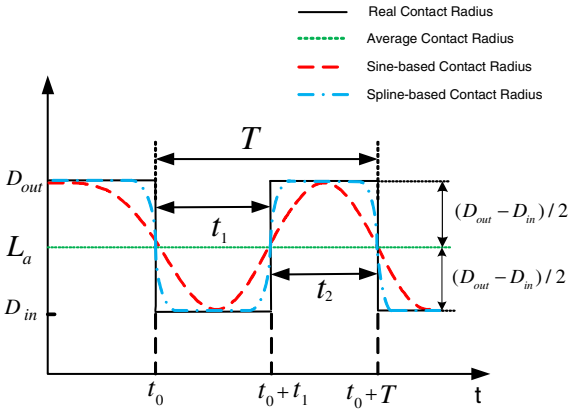

Fig. 5. The real the contact radius (solid black line), average contact radius (dotted green line), sinusoid (dashed red line) and spline (dash-dot blue line).

the motor torque constant, I_v is the robot moment of inertia around the robot mass center, I_0 is the combined moment of inertia of the motor, gear train and wheel referred to the motor shaft, b_0 is the combined viscous friction coefficient of the motor, gear and wheel and n is the gear reduction ratio.

It can be seen from (3) that, the contact radius L_i switches between the inner and outer wheel contact radius, i.e., between D_{in} and D_{out}. Therefore, each wheel has two contact modes and each contact mode corresponds to a smooth nonlinear dynamical subsystem. Therefore, a three-wheeled OMR based on MY wheels-II has eight contact modes in total. All of the contact modes are listed in Table I. When the robot moves with rotation, the robot is a switched nonlinear system because the robot dynamics switches between the subsystems. In addition, the switching signal of the switched nonlinear system is the wheel contact radius, i.e., $\mathbf{L} = \begin{bmatrix} L_1 & L_2 & L_3 \end{bmatrix}^T$. Furthermore, the robot is an autonomous switched nonlinear system.

C. Average Dynamic Model

Due to the fact that most of the control design methods are based on continuous dynamic models, the continuous dynamic modeling for the switch wheeled OMRs is desired. In our previous work, we proposed an average dynamic modeling method to derive the continuous dynamic model [1]. The average dynamic model can be easily derived by using the average contact radius L_a instead of the real contact radius in the discontinous dynamic mdoel (2); that is,

$$L_i = L_a = \frac{D_{out} + D_{in}}{2} \quad i = 1, 2, 3.$$

Obviously, one main advantage of the average dynamic model is that it is very easy to be obtained. The derived average dynamic model is smooth and nonlinear. In addition, the switching time is not required in this modeling method, i.e., the absolute encoder is unnecessary.

However, this modeling method now presents a problem. It can be seen from Fig. 5 (see the dotted green line) that the real contact radius in the subinterval $(t_0,\ t_0+t_1)$ and $(t_0+t_1,\ t_0+T)$ is D_{in} and D_{out}, respectively, whereas L_a is used as the contact radius in the average dynamic modeling method, resulting in the error of $\pm(D_{out}-D_{in})/2$ in the parameter L_i. In addition, this problem becomes much more pronounced especially when the following condition is not satisfied, producing large modeling errors:

$$\frac{L_m}{L_a} \ll 1 \tag{4}$$

where $L_m = \frac{D_{out}-D_{in}}{2}$. In other words, the real contact radius L_i can be considered as the nominal contact radius L_a with parameter variations. If the condition (4) is not satisfied, this means that there are large parameter variations of the nominal value L_a, resulting in large modeling errors.

Moreover, the condition (4) is equivalent to the following:

$$\gamma = \frac{D_{out} - D_{in}}{D_{in}} \ll 1 \tag{5}$$

In other words, the distance between the two small wheel sets (i.e., $D_{out} - D_{in}$) of the switch wheels should be quite small compared with the contact radius of the wheel to the center of gravity of the robot (i.e., D_{in} or D_{out}). For the mobile robot with large γ, significant modeling errors are produced in the average dynamic model. Therefore, more accurate continuous modeling method is expected, especially for the robots with large γ.

III. NLPV MODEL

In this section, we first derive the conditions leading to the wheel switching. Then based on the wheel switching conditions, a NLPV model is proposed for the robot.

A. Switching Conditions

According to (3), we define:

$$\begin{cases} \phi_{i0}^{in} = \phi_i - \frac{n\pi}{2} - \frac{\pi}{8} \\ \phi_{i0}^{out} = \phi_i - \frac{n\pi}{2} + \frac{\pi}{8} \end{cases} \tag{6}$$

In our previous study, we derived the conditions leading to the switching of the contact radius as follows:

(i) If the wheel rotates in one direction, i.e., forward or backward, the contact radius switches whenever the wheel turns $\frac{\pi}{4}$, i.e., $\phi_{i0}^{in} = \frac{\pi}{4}$ or $\phi_{i0}^{out} = \frac{\pi}{4}$ (Fig. 6).

(ii) If the wheel changes its direction of rotation, the turned angle of the wheel resulting in the switch depends the wheel angle position before changing the direction, i.e., ϕ_{0i}^{in} or ϕ_{0i}^{out} $(0 < \phi_{i0}^{in}, \phi_{i0}^{out} < \frac{\pi}{4})$ (Fig. 7).

Fig. 6 shows a wheel switching case of condition (i) when the wheel switches from the inner wheel contact to the outer wheel contact. Fig. 7 shows a wheel switching

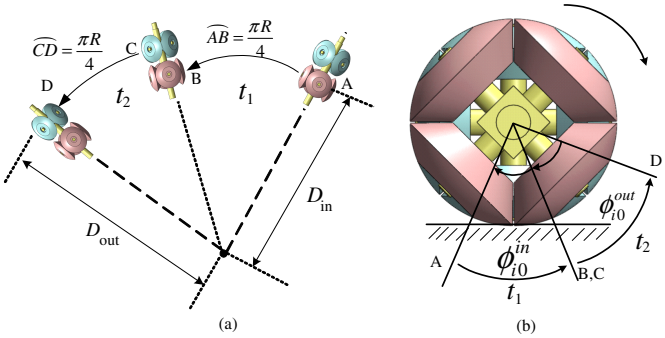

Fig. 6. Switching condition (i): (a) the top view, (b) the end view.

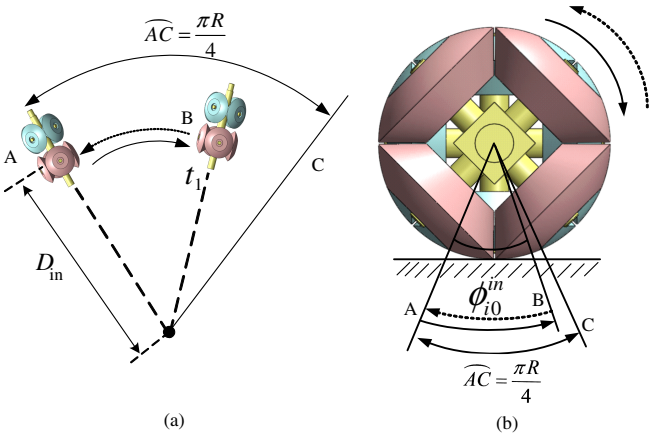

Fig. 7. Switching condition (ii): (a) the top view, (b) the end view.

case of condition (ii), when the change of the wheel rotation direction happens during the inner wheel contact. In other words, during the inner wheel contact with the ground, the wheel first moves along $\widehat{AB}$ in one direction. Then it changes the rotation direction and moves along $\widehat{BA}$.

B. NLPV Model

As analyzed before, the problem of average dynamic modeling method is that it produces a parameter error of $\pm L_m$ in the parameter L_i. Therefore, a more accurate dynamic model can be designed by reducing this parameter error. The key idea is to find a continuous curve to approach the real discontinuous contact radius D_{in} and D_{out} in the subinterval $(t_0,\, t_0+t_1)$ and $(t_0+t_1,\, t_0+T)$, respectively. Fig. 5 shows an example using sinusoid to approach the real contact radius (see the dashed red line). We can see that, compared with using the average contact radius L_a, the use of sinusoid to approach the real contact radius L_i produces much smaller parameter error. The NLPV model is derived by directly replacing the real discontinuous contact radius L_i in (2) with the continuous curve, such as sinusoid. Therefore, the NLPV model guarantees much better performance in predicting the behavior of the robot than the average dynamic model, even though the γ of the switch wheeled OMR is large.

The switching of the contact radius L_i is periodic only under special conditions, which can be derived by detailed analysis of the robot kinematics. The design of continuous curve to approximate the periodic switching of the contact radius is simple. However, in most cases, the switching of the contact radius is non-periodic. Therefore, the designed continuous curve should be adaptive to approach the non-periodic switching of the contact radius. Fortunately, this problem can be easily solved based on the derived switching conditions, regardless of periodic or non-periodic switching of the contact radius.

In the following, the adaptive sinusoid L_i^{NLPV} is designed to approach the discontinuous contact radius L_i. From the switching conditions (i) and (ii), it can be seen that the maximum wheel turned angle that leads to the switching of the contact radius is $\frac{\pi}{4}$, which is an essential property of the MY wheel-II mechanism. Therefore, the ϕ_{i0}^{in} and ϕ_{i0}^{out} can be used as the variable of the sinusoid L_i^{NLPV}. Since the switching of the contact radius between D_{in} and D_{out} is alternate, the period of the sinusoid is set as $\frac{\pi}{2}$. Then the adaptive sinusoid L_i^{NLPV} is easy to be obtained, and is given as follows:

$$L_i^{NLPV} = \begin{cases} L_a - L_m \sin(4\phi_{i0}^{in}) & if\ \ L_i = D_{in} \\ L_a + L_m \sin(4\phi_{i0}^{out}) & if\ \ L_i = D_{out} \end{cases} \tag{7}$$

where L_a and L_m are the same as those in (4).

The NLPV continuous dynamic model can be obtained by directly using the continuous sinusoid L_i^{NLPV} instead of the real discontinuous contact radius L_i in (2). The NLPV dynamic equations are not written here due to the limited space. In addition, the proposed NLPV model is easy to be implemented in the practice, because it only requires the real-time measure of the wheel rotation angle, which can be achieved by the mounted absolute encoder. Furthermore, L_i^{NLPV} can also be viewed as time-varying parameters, resulting in a nonlinear time-varying system.

In addition, the designed adaptive sinusoid L_i^{NLPV} is continuous. In the control of NLPV system, the bounded differential of L_i^{NLPV}, i.e., $\dot{L}_i^{NLPV}(t)$, is usually required [16]. It can be seen from (7) that the $\dot{L}_i^{NLPV}(t)$ is bounded. More importantly, all of the wheel switching cases, under either switching conditions (i) or (ii), are included in the designed sinusoid L_i^{NLPV}.

Remark 1: In addition to the sinusoid, various continuous curves, such as polynomial curves and spline, can be employed to approach the discontinuous contact radius based on the same idea presented above; that is, the ϕ_{i0}^{in} and ϕ_{i0}^{out} must be selected as variables in the curve expressions. Moreover, the NLPV modeling error based on sinusoid can be further reduced by using other continuous curves, such as polynomial curves or spline (see the dash-dot blue line in Fig. 5).

IV. SIMULATIONS

In this section, the effectiveness of the proposed NLPV model in predicting the behavior of the discontinuous dy-

namic model is verified through open-loop simulations. Since the proposed NLPV model has been derived from the discontinuous dynamic model, it only approaches the discontinuous dynamic model in terms of accuracy. In addition, the comparison with the average model is also conducted.

The following simulations were implemented in Matlab/Simulink. The parameter values used in the simulations are estimated from the robot prototype and are as follows: $m = 33$ kg, $I_v = 1.35$ kg$\cdot$m^2, $R = 0.06$ m, $D_{in} = 0.147$ m, $D_{out} = 0.236$ m, $I_0 = 9.7\times10^{-6}$ kg$\cdot$m^2, $k_t = 0.0292$N$\cdot$m/A, $k_b = 328$ rpm/V, $n = 150$, $b_0 = 6\times10^{-5}$ Nms/rad, $R_a = 0.61\,\Omega$.

Model validation is usually conducted by comparing the responses of different models under the same control input [17]. Thereby, we give the same control input to the three models, i.e., discontinuous model, average model and NLPV model, respectively. In order to show the effectiveness of the adaptive sinusoid L_i^{NLPV} in approaching the non-periodic switching of the contact radius, the following time-varying control input $u(t) = \begin{bmatrix} u_1(t) & u_2(t) & u_3(t) \end{bmatrix}^T$ V is selected:

$$u_1(t) = 10\sin(0.2t)$$
$$u_2(t) = 20\cos(0.2t)$$
$$u_3(t) = 20\sin(0.4t)$$

Simulation results are shown in Fig. 8 - Fig. 14. It is observed from Fig. 8 that, the designed sinusoid contact radius is able to approach the real discontinuous contact radius, even though the switching of the real contact radius is non-periodic.

In addition, responses of the three models, i.e., robot position and velocity, are depicted in Fig. 9 - Fig. 14. It should be noted that our robot platform is with large γ, i.e., $\gamma = 0.61$. As seen in Fig. 9 - Fig. 14, the responses of the average dynamic model certainly have large estimation errors against the responses produced by the discontinuous dynamic model. This is because the robot configuration does not meet the requirement in (5), and thus the average dynamic modeling method produces large modeling errors. However, it is observed that the responses of the proposed NLPV model are in excellent agreement with the responses produced by the discontinuous dynamic model. Therefore, compared with the average dynamic model method, the proposed NLPV model shows definitely much better performance in approaching the responses produced by the discontinuous model, even though for the robot with large γ.

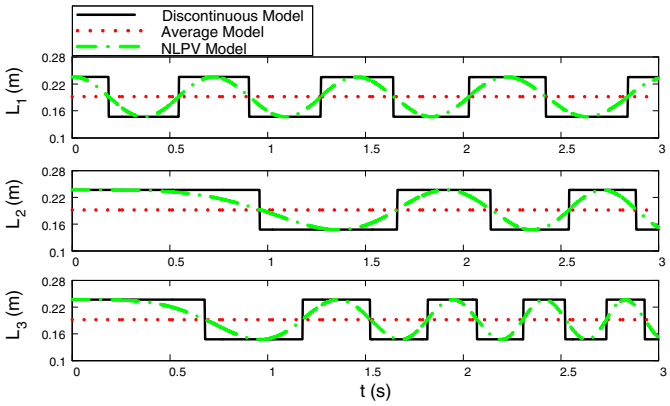

Fig. 8. Wheel contact radius in the three models: real contact radius L_i, average contact radius L_a and sinusoid contact radius L_i^{NLPV}.

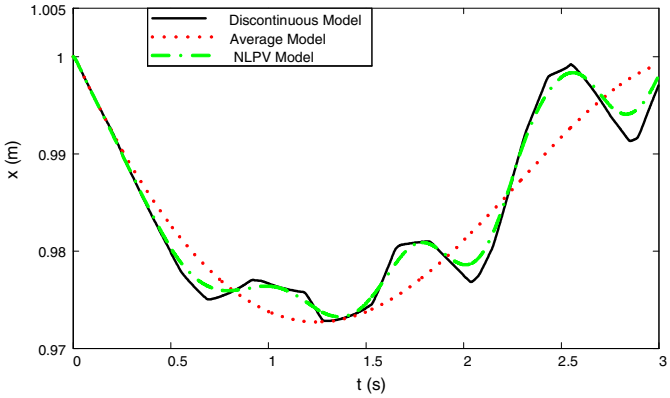

Fig. 9. Open-loop simulation results: robot position in x component.

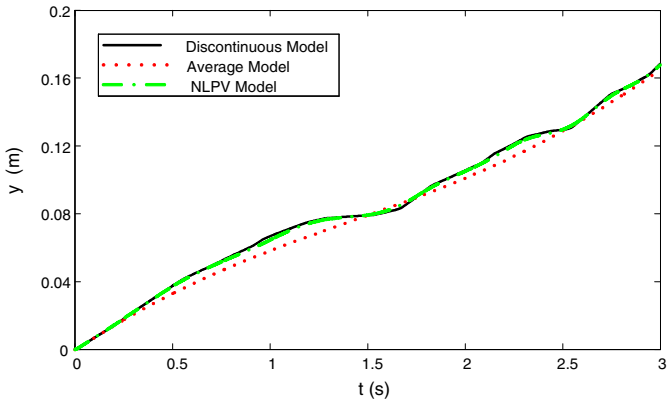

Fig. 10. Open-loop simulation results: robot position in y component.

V. CONCLUSIONS

In this paper, we have derived a NLPV dynamic model from a given discontinuous dynamic model, for a three-wheeled OMR based on MY wheels-II. The proposed model is simple but effective in approaching the responses produced by the discontinuous dynamic model, regardless of the configurations of the robot. Firstly, we have analyzed the problems in the average dynamic model, which showed that the average dynamic model is only effective for robots under a certain class of the configurations. Based on the derived switching conditions of the MY wheel-II, a simple NLPV dynamic model was proposed to overcome the problems in the average dynamic model. The key idea is to design adaptive continuous curves to approach the real discontinuous contact radius. Open-loop simulations verified the effectiveness of the proposed NLPV modeling method against the discontinuous dynamic model, as well as the average model. The proposed NLPV model achieves much better performance than the average dynamic model.

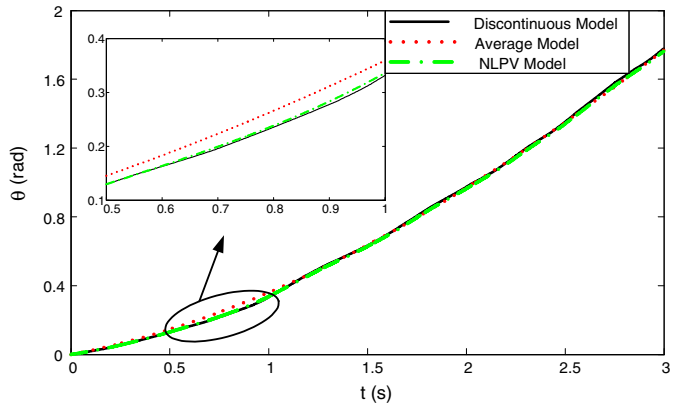

Fig. 11. Open-loop simulation results: robot orientation θ.

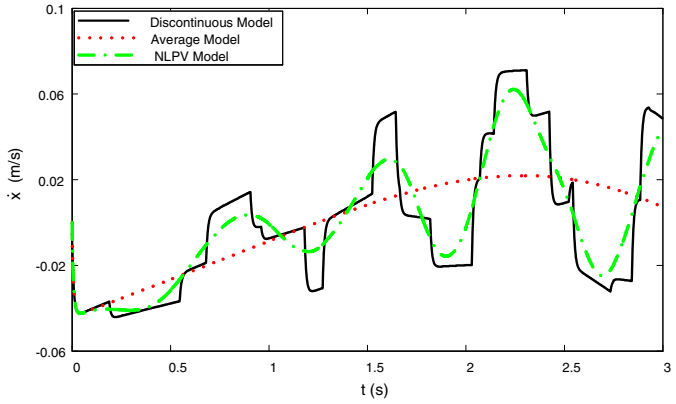

Fig. 12. Open-loop simulation results: robot velocity in x component.

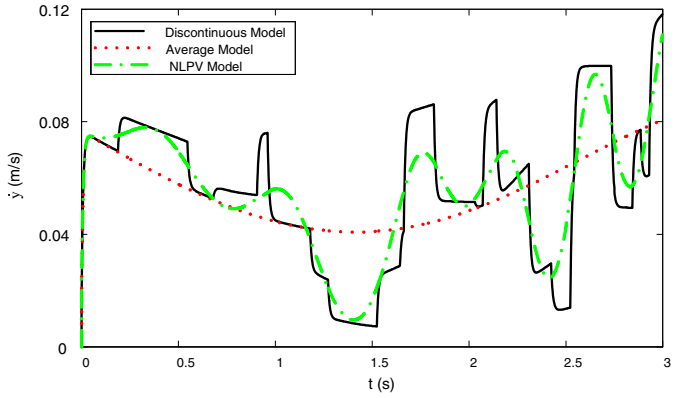

Fig. 13. Open-loop simulation results: robot velocity in y component.

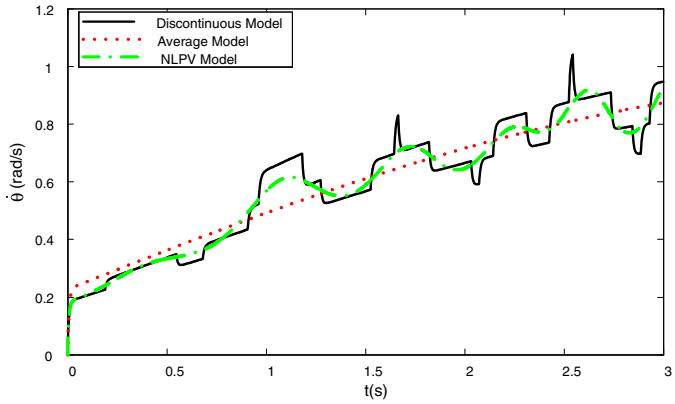

Fig. 14. Open-loop simulation results: robot rotational velocity $\dot{\theta}$.

References

[1] C. Ren and S. Ma, "Dynamic modeling and analysis of an omnidirectional mobile robot," in *Intelligent Robots and Systems (IROS), 2013 IEEE/RSJ International Conference on*. IEEE, 2013, pp. 4860–4865.

[2] B. Ilou, "Wheels for a course stable self-propelling vehicle movable in any desired direction on the ground or some other base," Patent U.S. Patent 3 876 255, Apr 8, 1975.

[3] K.-S. Byun and J.-B. Song, "Design and construction of continuous alternate wheels for an omnidirectional mobile robot," *J. Robot. Syst.*, vol. 20, no. 9, pp. 569–579, 2003.

[4] K. Tadakuma and R. Tadakuma, "Mechanical design of "omni-ball": Spherical wheel for holonomic omnidirectional motion," in *Proc. IEEE Int. Conf. Automation Sci. Eng. (CASE)*, Sept. 2007, pp. 788 –794.

[5] M. Wada and H. Asada, "Design and control of a variable footprint mechanism for holonomic omnidirectional vehicles and its application to wheelchairs," *IEEE Trans. Robot. Autom.*, vol. 15, no. 6, pp. 978 –989, Dec. 1999.

[6] F. Pin and S. Killough, "A new family of omnidirectional and holonomic wheeled platforms for mobile robots," *IEEE Trans. Robot. Autom.*, vol. 10, no. 4, pp. 480 –489, Aug. 1994.

[7] C. Ye and S. Ma, "Development of an omnidirectional mobile platform," in *Proc. IEEE Int. Conf. Mechatronics and Automation (ICMA)*, Changchun, China, Aug. 2009, pp. 1111 –1115.

[8] S. Ma, C. Ren, and C. Ye, "An omnidirectional mobile robot: Concept and analysis," in *Proc. IEEE Int. Conf. Robotics and Biomimetics (ROBIO)*, Guangzhou, China, 2012, pp. 920–925.

[9] G. Indiveri, "Swedish wheeled omnidirectional mobile robots: Kinematics analysis and control," *IEEE Trans. Robot.*, vol. 25, no. 1, pp. 164 –171, Feb. 2009.

[10] H. Asama *et al*, "Development of an omni-directional mobile robot with 3 dof decoupling drive mechanism," in *Proc. IEEE Int. Conf. Robotics and Automation (ICRA)*, vol. 2, 1995, pp. 1925–1930.

[11] J.-L. Wu, "Feedback stabilization for multiinput switched nonlinear systems: two subsystems case," *IEEE Trans. Autom. Control*, vol. 53, no. 4, pp. 1037–1042, 2008.

[12] R. Ma and J. Zhao, "Backstepping design for global stabilization of switched nonlinear systems in lower triangular form under arbitrary switchings," *Automatica*, vol. 46, no. 11, pp. 1819 – 1823, 2010.

[13] M. Branicky, V. Borkar, and S. Mitter, "A unified framework for hybrid control: model and optimal control theory," *IEEE Trans. Autom. Control*, vol. 43, no. 1, pp. 31–45, 1998.

[14] K. Watanabe, Y. Shiraishi, S. Tzafestas, J. Tang, and T. Fukuda, "Feedback control of an omnidirectional autonomous platform for mobile service robots," *J. Intell. Robot. Syst.*, vol. 22, pp. 315–330, 1998.

[15] Y. Liu, J. J. Zhu, R. L. W. II, and J. Wu, "Omni-directional mobile robot controller based on trajectory linearization," *Robot. Auton. Syst.*, vol. 56, no. 5, pp. 461 – 479, 2008.

[16] M. Sznaier and J. Cloutier, "Model predictive control of nonlinear parameter varying systems via receding horizon control lyapunov functions," *IEE CONTROL ENGINEERING SERIES*, pp. 81–106, 2001.

[17] J. Martins, Z. Mohamed, M. Tokhi, J. S. da Costa, and M. Botto, "Approaches for dynamic modelling of flexible manipulator systems," *IEE Proc. Contr. Theory Appl.*, vol. 150, no. 4, pp. 401–411, 2003.